Design Procedure for Output Current Control and Damping Control of Matrix Converter

Hiroki Takahashi and Jun-ichi Itoh
Dept. of Energy and Environmental Science
Nagaoka University of Technology
Nagaoka, Niigata, Japan
thiroki@stn.nagaokaut.ac.jp and itoh@vos.nagaokaut.ac.jp

***Abstract*— This paper presents a design procedure for an output current control and an output damping control of a matrix converter to suppress LC filter resonance and improve transient current response. With a conventional design method which gives preference to stability, the output damping control causes a large output current overshoot and a control bandwidth of the output current is affected. Therefore, in order to obtain a desired transient response keeping a stable operation, this paper describes a modified control block diagram which a reference filter is added in to suppress the output current overshoot and a detailed design procedure using Bode-diagrams and a flowchart. From the experimental results, the output damping control designed with the proposed method suppresses the filter resonance, which results in stable operation. In addition, the proposed design method reduces the output current overshoot of 60% and an error between the desired and the obtained control bandwidth in comparison with the conventional method in experiments.**

Keywords*— Matrix converter, Resonance, Damping control

I. INTRODUCTION

Recently, a matrix converter has attracted a lot of attentions as an interface converter of a wind turbine system and an elevator because this converter has no DC energy buffer such as bulky electrolytic capacitors [1]-[6]. A matrix converter promises to achieve higher efficiency, smaller size and longer life-time compared to a conventional BTB (back to back) system which consists of a PWM rectifier and a PWM inverter.

A matrix converter requires LC filters in the grid side to eliminate harmonic current due to switching operation. However, a matrix converter has a problem that a filter LC resonance is excited by a grid voltage fluctuation and an input current fluctuation. In general, the filter resonance is suppressed by using damping resistors connected in parallel with the filter inductors [7]. However, when a transformer is connected to the input side of the matrix converter such as a wind turbine system and an elevator which requires isolation between a load and the grid, a leakage inductance of the transformer is used as the filter inductors and the damping resistors are not inserted. Therefore, a suppression method for the filter resonance is needed.

In past works, some papers about stability analysis of a matrix converter to prevent the filter resonance have been presented [8]-[11]. These papers investigate the stability taking account into a detection of the input voltage with a filter [8], digital control [9]-[10] and matrix converter losses [10]. In addition, an approach to the stability based on admittance of a matrix converter has reported [11]. These investigations clarify stable limitations of a matrix converter operation with each method and suppress the filter resonance. However, the stability of a matrix converter can be improved more from the point of view of a current control of a matrix converter.

As control strategies to suppress the filter resonance, damping controls have been proposed [12]-[14]. The damping controls are separated into two types. The first one is a damping control combined with the input current control of the matrix converter [12]-[13] and another one is combined with the output current control [14]. Then, the output damping control has an advantage when the matrix converter is applied to a wind farm and an elevator which requires a field oriented control for accurate speed control. The advantage is that a required feedback control is on the output stage only while the matrix converter with the input damping control needs feedback loops on both of the input and the output sides.

The authors have already proposed the output damping control and its parameter design method [15]. The presented design method is based on a gain margin of the matrix converter and suppresses the filter resonance. However, the damping control designed with the conventional method based on the gain margin generates a large overshoot of the output current. Furthermore, a detailed design procedure to earn an intended control bandwidth of the output current has not been presented.

This paper proposes a modified control block diagram and a design procedure for the output current control and the output damping control to suppress the output current overshoot and to obtain an intended control bandwidth. The output current overshoot is reduced by an added reference filter for pole-zero cancellation and designed with an approximate model of the matrix converter. Moreover, a desired control bandwidth of the output current and a stable operation are achieved by a proposed design flowchart based on Bode-diagrams. The proposed reference filter and the design procedure result in fine output performance compared with the conventional

method. This paper is organized as follows; firstly, an integrated block model and an approximate model of the matrix converter to design the output damping control and the output current control including the reference filter are described; secondly, the design flowchart for the controls is presented; finally, the stability and the transient response are evaluated in simulation and experiment.

II. System Configuration

Fig. 1 shows a system block diagram of the matrix converter with the output damping control. For simplicity, the input transformer is assumed as an ideal transformer and a leakage inductance L_f, and the ideal transformer is omitted. For the same reason, a load motor is replaced with an R-L load. In addition, an output current control with a PI controller is used because a wind turbine system and an elevator require a field oriented control for accurate speed control. The output damping control which has a damping gain K_d and a damping HPF (high pass filter) of a time constant T_{hpf} is combined with the output current control feedback and suppresses the filter resonance. However, the output damping control generates a large current overshoot in a transient state because a closed-loop transfer function of the output current control has a zero due to the damping control. Hence, a reference filter F(s) is added for a pole-zero cancellation. In order to derive an appropriate equation of F(s) and obtain an intended control bandwidth and a stable operation, this paper deals with Bode-diagrams derived from an integrated block model which is composed of a main circuit and a control diagram. Moreover, a design procedure for the output damping control and the output current control is proposed.

III. Design Model

A. Modeling of Matrix Converter based on Space Vector

In order to derive the integrated block model of a matrix converter, an output voltage and an input current equations are required. Then, these equations of a matrix converter based on the duty-cycle space vector have been presented [16]. In this paper, the integrated block model of the matrix converter which is composed of the main circuit and the control diagram is derived by using the duty-cycle space vector.

Fig. 2 shows the integrated block model of the matrix converter. Variables in bold font represent their space vectors. For example, an input voltage vector $\boldsymbol{v_{in}}$ is defined as following.

$$\boldsymbol{v_{in}} = \frac{2}{3}\left(v_r + v_s e^{j\frac{2}{3}\pi} + v_t e^{-j\frac{2}{3}\pi} \right) \quad (1)$$

where, v_r is the input R-phase voltage, v_s is the input S-phase voltage and v_t is the input T-phase voltage.

In order to connect the input and the output circuits of the matrix converter, the duty-cycle space vector $\boldsymbol{m_d}$ and

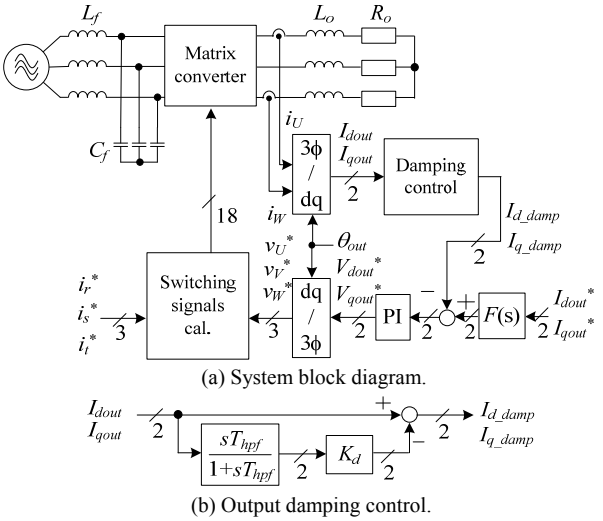

Fig. 1. Matrix converter with the output damping control to suppress the filter resonance and the proposed reference filter F(s) to reduce the output current overshoot.

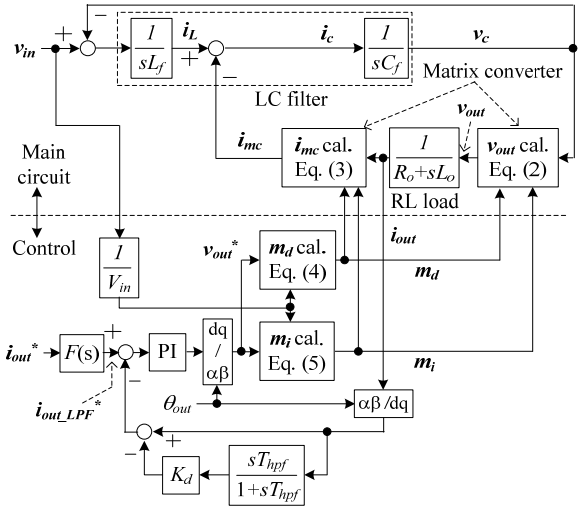

Fig. 2. Integrated block model of the matrix converter which is composed of the main circuit and the control diagram. This block diagram is based on the duty-cycle space vector.

$\boldsymbol{m_i}$ are introduced. Then, an output voltage vector $\boldsymbol{v_{out}}$ and an input current vector $\boldsymbol{i_{mc}}$ are yielded by (2) and (3).

$$\boldsymbol{v_{out}} = \frac{3}{2}\overline{\boldsymbol{m_i}}\boldsymbol{v_c} + \frac{3}{2}\boldsymbol{m_d}\overline{\boldsymbol{v_c}} \quad (2)$$

$$\boldsymbol{i_{mc}} = \frac{3}{2}\boldsymbol{m_i}\boldsymbol{i_{out}} + \frac{3}{2}\boldsymbol{m_d}\overline{\boldsymbol{i_{out}}} \quad (3)$$

where, $\boldsymbol{v_c}$ is a filter capacitor voltage vector and $\boldsymbol{i_{out}}$ is an output current vector. Note that a bar placed over a variable indicates complex conjugate. In contrast, $\boldsymbol{m_d}$ and $\boldsymbol{m_i}$ are represented by follows.

$$\boldsymbol{m_d} = \frac{\boldsymbol{v_{in}}}{3V_i}\boldsymbol{v_{out}}^* \quad (4)$$

$$\boldsymbol{m_i} = \frac{\boldsymbol{v_{in}}}{3V_i}\overline{\boldsymbol{v_{out}}^*} \quad (5)$$

where, $\boldsymbol{v}_{out}^{*}$ is an output voltage reference vector and V_i is amplitude of the input voltage.

However, (2) and (3) are non-linear equations because time constants of fluctuation of $\boldsymbol{v}_c$, $\boldsymbol{m}_d$, $\boldsymbol{m}_i$ and $\boldsymbol{i}_{out}$ are close to each other. Therefore, a linear approximation method around a steady operating point is applied to these non-linear parts in order to draw Bode-diagrams. Equations (2) to (5) are separated into steady and differential components, and the differential components are expressed as (6) to (9).

$$\Delta \boldsymbol{v}_{out} = \frac{3}{2}\left(\overline{\Delta \boldsymbol{m}_i}\boldsymbol{v}_{cs} + \overline{\boldsymbol{m}_{is}}\Delta \boldsymbol{v}_c\right) + \frac{3}{2}\left(\Delta \boldsymbol{m}_d\,\overline{\boldsymbol{v}_{cs}} + \boldsymbol{m}_{ds}\,\overline{\Delta \boldsymbol{v}_c}\right) \quad (6)$$

$$\Delta \boldsymbol{i}_{mc} = \frac{3}{2}\left(\Delta \boldsymbol{m}_i \boldsymbol{i}_{outs} + \boldsymbol{m}_{is}\Delta \boldsymbol{i}_{out}\right) + \frac{3}{2}\left(\Delta \boldsymbol{m}_d\,\overline{\boldsymbol{i}_{outs}} + \boldsymbol{m}_{ds}\,\overline{\Delta \boldsymbol{i}_{out}}\right) \quad (7)$$

$$\Delta \boldsymbol{m}_d = \frac{\boldsymbol{v}_{ins}}{3V_i}\Delta \boldsymbol{v}_{out}^{*} \quad (8)$$

$$\Delta \boldsymbol{m}_i = \frac{\boldsymbol{v}_{ins}}{3V_i}\overline{\Delta \boldsymbol{v}_{out}^{*}} \quad (9)$$

where, suffix "s" represents the steady component based on its fundamental frequency while "Δ" means the differential component in a transient state. It should be noted that $\Delta \boldsymbol{v}_{in}$ is not considered because the output current response is evaluated in this paper.

Fig. 3 shows a linearized block model of the matrix converter regarding the differential components. Frequency characteristics of the output current control and the stability are obtained by using Bode-diagram. Note that analyses should be implemented with DC mode in which an input and an output angles are fixed because a rotating frequency of the steady vector does not equal to a rotating frequency of the differential vector.

B. Verification of the linearized model with simulation

Table 1 and Table 2 present the main circuit and the control parameters of the circuit model as illustrated in Fig. 1 and the linearized model as shown in Fig. 3. This section shows a simulation result without the output current control and the output damping control in order to evaluate a verification of the linearized model. Note that the inductor and capacitor parameters are normalized based on 50 Hz. In addition, a carrier frequency is increased to 100 kHz in this section only.

Fig. 4 shows an indicial response of the circuit model and the linearized model with an open-loop control in a simulation. It should be noticed that all waveforms are applied with a 1 kHz cut-off frequency LPF (low pass filter) in order to observe these average waveform without switching ripples. From Fig. 4, it is confirmed that the linearized model waveforms correspond to the circuit model result. Furthermore, error between the circuit model and the linearized model waveforms is less than 1% in a steady state. Thus, the linearized model is valid for modeling of the matrix converter. In consequence, the output current control including the proposed reference filter and the output damping control are designed with Bode-diagrams derived from the linearized model in the next chapter.

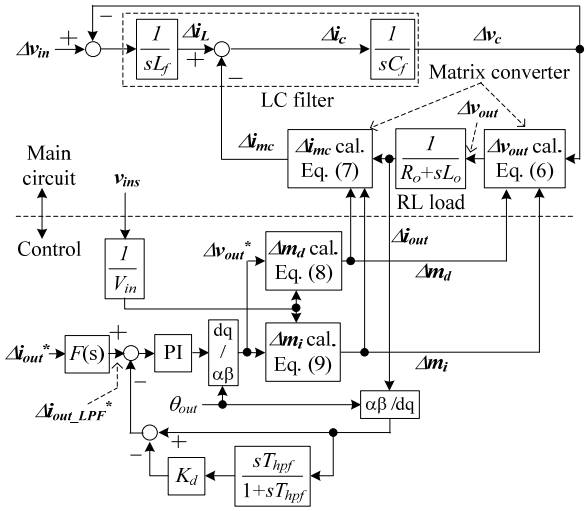

Fig. 3. Linearized block model of the matrix converter focusing on the differential components. Stability and a control bandwidth of the output current are evaluated by analyzing this block model.

TABLE 1. CIRCUIT PARAMETERS OF THE MATRIX CONVERTER

Input line voltage	200 V	Rated output voltage	173 V
Rated power	3 kW	Carrier frequency	10 kHz
Input filter L (L_f)	10.0 mH (23.6%)	Load resistance (R_o)	12.7 Ω (127%)
Input filter C (C_f)	4.55 μF (1.91%)	Load inductance (L_o)	6.27 mH (19.7%)
Input voltage angle	105 deg.	Output voltage angle	15 deg.

TABLE 2. CONTROL PARAMETERS FOR OPEN-LOOP CONTROL

Open-loop control	d-axis voltage command (steady state)	0.5 p.u.
	d-axis voltage command (step input)	0.01 p.u.
	q-axis voltage command (steady state)	0 p.u.
	q-axis voltage command (step input)	0 p.u.

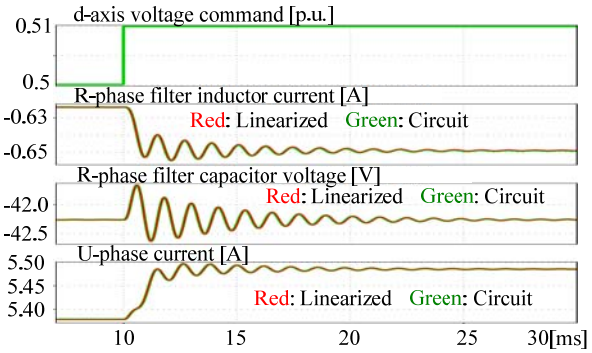

Fig. 4. Indicial response of the circuit model and the linearized model with an open-loop control in a simulation. It is confirmed that the linearized model result corresponds to the circuit model result.

IV. Proposed Design Procedure of Control Parameters

A. Approximate Model to Design Proposed Reference Filter and Control Parameters

In order to design the output current control with the proposed reference filter and the output damping control, Bode-diagrams of the linearized block model in Fig. 3 should be clarified. However, the linearized block model is a fifth order transfer function, which is caused by the input LC filter, the load inductor, the PI controller and the output damping control, and the transfer function is very complicated. Therefore, an approximate model based on a third order transfer function is used to design these controls.

Fig. 5 shows the approximate block model between $\Delta \boldsymbol{i}_{\mathbf{out\_LPF}}{}^{*}$ and $\Delta \boldsymbol{i}_{\mathbf{out}}$ in Fig. 3 without the output damping control. The approximate model is based on the gain curve of the linearized block model in Fig. 3 in order to obtain the proposed reference filter configuration easily. It should be noted that the output damping control is not applied when a forward transfer function in the approximate model is calculated. The approximate model is a second order transfer function which has a damping factor ζ and a natural angular frequency ω_n. The transfer function in Fig. 5 approximates a resonance point characteristic of the linearized block model. Therefore, ζ and ω_n are expressed by (10) and (11).

$$\zeta = \sqrt{\frac{1}{2} - \frac{1}{2}\sqrt{1 - \frac{1}{M_p{}^2}}} \qquad (10)$$

$$\omega_n = \omega_p \left(1 - 1/M_p{}^2\right)^{\frac{1}{4}} \qquad (11)$$

where, M_p is a peak gain of the resonance point and ω_p is a resonance angular frequency which are measured with the gain characteristic of the linearized block model of the matrix converter in Fig. 3.

Table 3 shows parameters of the PI controller. These parameters should be designed with a flowchart as presented in the next section. However, in order to clarify the validity of the approximate block model in Fig. 5, the PI parameters are set to the linearized model in Fig. 3.

Fig. 6 shows a gain characteristic of the closed-loop transfer function between $\Delta \boldsymbol{i}_{\mathbf{out\_LPF}}{}^{*}$ and $\Delta \boldsymbol{i}_{\mathbf{out}}$ without the output damping control. From Fig. 6, the resonance peak gain and the resonance frequency of the approximate model designed with (10) and (11) corresponds to the linearized block model of the matrix converter. In addition, the gain characteristic of the approximate model is similar to the linearized model. In a frequency region higher than 1 kHz, gain error between the linearized model and the approximate model can be neglected because the region is not available for the current control due to detection delay and PWM delay of the real system if the carrier frequency is set to 10 kHz as shown in Table 1. Thus, the approximate model in Fig. 6 is valid for the

Fig. 5. Approximate block model between $\Delta \boldsymbol{i}_{\mathbf{out\_LPF}}{}^{*}$ and $\Delta \boldsymbol{i}_{\mathbf{out}}$ without the output damping control to simplify the design procedure. The transfer function of this block diagram becomes the standard form of the second order system.

TABLE 3. PARAMETERS OF THE PI CONTROLLER

PI controller	Current command (step input)	0.01 p.u.
	Current command (steady state)	0.4 p.u.
	ACR natural frequency	650 Hz

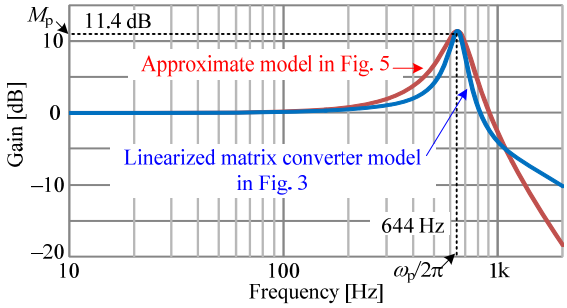

Fig. 6. Gain characteristic of the closed-loop transfer function between $\Delta \boldsymbol{i}_{\mathbf{out\_LPF}}{}^{*}$ and $\Delta \boldsymbol{i}_{\mathbf{out}}$ without the output damping control. The gain curve of the approximate model is similar to the linearized model.

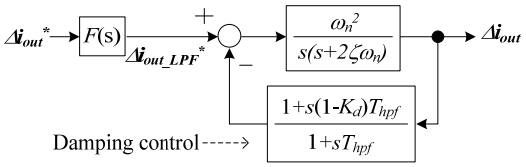

Fig. 7. Approximate block model between $\Delta \boldsymbol{i}_{\mathbf{out}}{}^{*}$ and $\Delta \boldsymbol{i}_{\mathbf{out}}$ taking the output damping control into account. The proposed reference filter $F(s)$ is derived from this block model.

modeling of the linearized block model of the matrix converter without the output damping control.

Fig. 7 shows the approximate block model between $\Delta \boldsymbol{i}_{\mathbf{out}}{}^{*}$ and $\Delta \boldsymbol{i}_{\mathbf{out}}$ taking the output damping control into account. First, a transfer function of the proposed reference filter $F(s)$ to suppress the output current overshoot is derived. A closed-loop transfer function between $\Delta \boldsymbol{i}_{\mathbf{out\_LPF}}{}^{*}$ and $\Delta \boldsymbol{i}_{\mathbf{out}}$ is presented by (12).

$$\frac{\Delta i_{out}}{\Delta i_{out\_LPF}{}^{*}} = \frac{\frac{\omega_n{}^2}{T_{hpf}}\left(1+sT_{hpf}\right)}{s^3 + \left(\frac{1}{T_{hpf}} + 2\zeta\omega_n\right)s^2 + \omega_n\left(\frac{2\zeta}{T_{hpf}} + \omega_n\left(1-K_d\right)\right)s + \frac{\omega_n{}^2}{T_{hpf}}} \qquad (12)$$

It is obvious that the output damping control generates a large current overshoot because the closed-loop transfer function between $\Delta \boldsymbol{i}_{\mathbf{out\_LPF}}{}^{*}$ and $\Delta \boldsymbol{i}_{\mathbf{out}}$ has a zero depending on T_{hpf}. In order to suppress the output current overshoot, the zero in (12) should be cancelled. Hence, $F(s)$ is defined as (13).

$$F(s) = \frac{1}{1+sT_{hpf}} \qquad (13)$$

Hence, the proposed reference filter is designed easily when the T_{hpf} is decided in the proposed design procedure.

B. Design Flowchart

In order to design the output current control and the output damping control, this section proposes a design flowchart.

Fig. 8 shows a proposed design flowchart for the output current control and the output damping control to ensure a desired control bandwidth and the stability. Input parameters into the flowchart are determined by specifications and outputs of the flowchart are the proportional gain K_p, the integral time T_i of the PI controller, K_d and T_{hpf} of the output damping control.

1) Step 1: Calculation of K_p and T_i of PI Controller

First, K_p and T_i should be calculated in order to draw a Bode-diagram as shown in Fig. 6. Then, K_p and T_i are designed by (14) and (15), supposing that a plant of the controller is an R-L model.

$$K_p = \omega_{c\_design} L_o \tag{14}$$

$$T_i = \frac{L_o}{R_o} \tag{15}$$

where, ω_{c_design} is a desired cut-off angular frequency of the output current control. It should be noted that the design concept of (14) and (15) is based on the first order transfer function of the output current control loop neglecting the input LC filter and the output damping control. However, the actual cut-off angular frequency is changed by the resonance characteristic and the output damping control.

2) Step 2: Simulation to Measure M_p and ω_p

In order to calculate parameters of the approximate model for a simple design process, a Bode-diagram between $\Delta \boldsymbol{i}_{\mathbf{out\_LPF}}{}^{*}$ and $\Delta \boldsymbol{i}_{\mathbf{out}}$ of the linearized matrix converter block model such as Fig. 6 is drawn by a simulator. In this paper, Piece-wise Linear Electrical Circuit Simulation (PLECS) is used as a simulator.

3) Step 3: Calculation of ζ and ω_n

In order to obtain the approximate model of the matrix converter, ζ and ω_n are calculated by (10) and (11).

4) Step 4: Decision of K_d and T_{hpf}

By using (12) and (13), a Bode-diagram between $\Delta \boldsymbol{i}_{\mathbf{out}}{}^{*}$ and $\Delta \boldsymbol{i}_{\mathbf{out}}$ of the approximate block model in Fig. 7 is illustrated. Then, K_d and T_{hpf} is decided with the Bode-diagram to earn an intended control bandwidth of the output current.

Fig. 9 shows gain characteristics between $\Delta \boldsymbol{i}_{\mathbf{out}}{}^{*}$ and $\Delta \boldsymbol{i}_{\mathbf{out}}$ of the approximate block model when the K_d and f_{hpf} are changed respectively. Note that f_{hpf} is a cut-off frequency of a HPF of the output damping control. Fig. 9 (a) shows a gain characteristic when K_d is changed and f_{hpf} is a constant of 50 Hz, and (b) shows a result when f_{hpf} is changed and K_d is a constant of 0.5 p.u.. From Fig. 9 (a), the cut-off frequency of the output current control increases as K_d is increased from 0.3 p.u. to 0.6 p.u.. However, the cut-off frequency is decreased in the region where K_d is over 0.6 p.u.. This is affected the characteristic around the resonance point. On the other hand, it is confirmed that the cut-off frequency increases as the f_{hpf} is increased from Fig. 9 (b). Therefore, an intended control bandwidth of the output current is yielded by adjusting the damping parameters K_d and f_{hpf}.

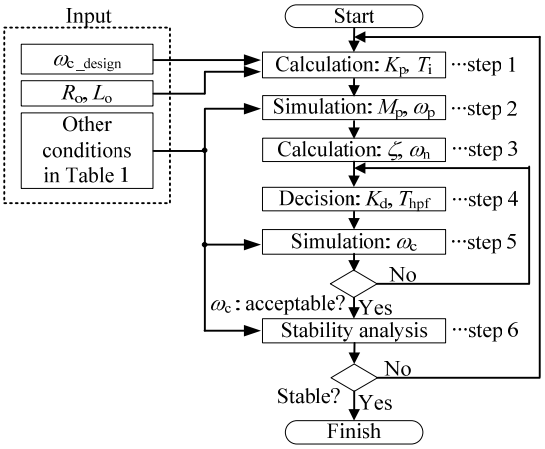

Fig. 8. Proposed design flowchart for the output current control and the output damping control.

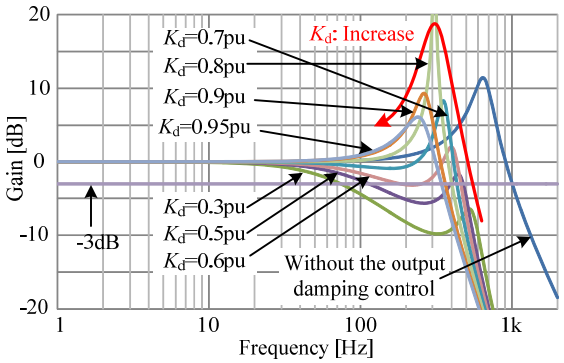

(a) K_d is changed (f_{hpf} is a constant of 50 Hz).

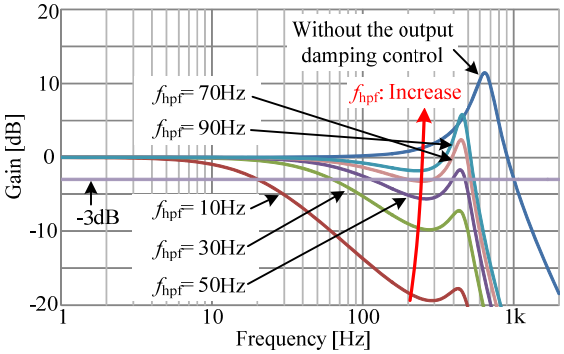

(b) f_{hpf} is changed (K_d is a constant of 0.5 p.u.).

Fig. 9. Gain characteristics between $\Delta \boldsymbol{i}_{\mathbf{out}}{}^{*}$ and $\Delta \boldsymbol{i}_{\mathbf{out}}$ of the approximate block model when the K_d and f_{hpf} are changed respectively.

5) Simulation to Confirm Cut-off Frequency of Output Current Control

A Bode-diagram between $\Delta \boldsymbol{i}_{\mathbf{out}}{}^{*}$ and $\Delta \boldsymbol{i}_{\mathbf{out}}$ of the linearized block model in Fig. 3 with the decided damping parameters is drawn and the control bandwidth

of the output current ω_c is evaluated. If the obtained control bandwidth is not acceptable, the damping parameters should be redesigned by going back to Step 4.

6) Stability Analysis

Finally, the stability of the system is analyzed with a Nyquist-diagram. If the obtained stability does not satisfy the specification of stability, the PI parameters and the damping parameters which influence the frequency characteristic of the open-loop transfer function of the output current control should be adjusted again. For example, ω_{c_design} is reduced or T_{hpf} is increased from the original value in order to increase the stability and K_d is redesigned to earn the intended control bandwidth.

V. Comparison Results between the Proposed and Conventional Methods in Simulation

Table 4 presents the designed parameters of the output damping control with the proposed design flowchart in Fig. 8 and the conventional method. It should be noted that the conventional method is based on the desired gain margin [15]. In the conventional method, the PI parameters are designed with (14) and (15) in common with the proposed procedure. In addition, the damping parameters are calculated by the following equations.

$$(g_a + g_m) + 20\log_{10}(1 - K_d) = 0 \quad (16)$$

$$T_{hpf} = \frac{5}{2\pi(1 - K_d) f_{cp}} \quad (17)$$

where, f_{cp} is a phase-crossover frequency of a gain curve of the output current control without the output damping control, g_a is a gain at f_{cp} without the damping control and g_m is a desired gain margin which is set to the same as the designed result with the proposed method for comparison.

Fig. 10 shows gain characteristics between $\Delta \boldsymbol{i}_{\mathbf{out}}^*$ and $\Delta \boldsymbol{i}_{\mathbf{out}}$ with the proposed and the conventional methods. The gain curve of the approximate model meets -3 dB at 650 Hz as shown in Table 3 by the proposed design flowchart. In addition, the proposed method mitigates error between the desired and the obtained cut-off frequencies by 1/4 in comparison with the conventional method. This is because the conventional method gives preference to the stability design over adjusting the control bandwidth. Moreover, the gain curve with the conventional method increases in the region around 100 Hz because of the zero generated by the output damping control and causes a large output current overshoot.

Fig. 11 shows the Nyquist-diagram of the linearized block model of the matrix converter between $\Delta \boldsymbol{i}_{\mathbf{out\_LPF}}^*$ and $\Delta \boldsymbol{i}_{\mathbf{out}}$ with the proposed and the conventional procedures. As a result of the proposed procedure, the Nyquist-diagram of the proposed method has a gain margin of 3.85 dB and the system is stable, which is equivalent to suppression of the filter resonance. It should be noticed that the experimental setup has more stability because the loss of the matrix converter behaves as a damping resistor [10]. On the other hand, the conventional method also stabilizes the system with the gain margin of 4.30 dB. Then, error of the gain margin between the intended value of 3.85 dB and the actual is caused by the break point approximation of a Bode-diagram for deriving (17) [15]. Therefore, it is confirmed that the proposed procedure yields the stability and the desired control bandwidth of the output current.

Fig. 12 shows the output d-axis current waveform in simulations with the linearized block model in Fig. 3. From Fig. 12 (a), the system without the damping control becomes unstable right after the step input because the system gain margin is -3.20 dB as shown in Fig. 11. However, the output damping control designed with the proposed and the conventional methods stabilizes the system. Then, the proposed method reduces the d-axis current overshoot by 67% because of the proposed reference filter $F(s)$ in comparison with the conventional method. Hence, it is confirmed that the proposed method achieves less overshoot of the output current than the conventional method in the simulations.

TABLE 4. Designed Parameters of the Output Damping Control.

Proposed method	Damping gain (K_d)	0.60 p.u.
	Damping HPF time constant (T_{hpf})	0.64 ms
Conventional method	Damping gain (K_d)	0.56 p.u.
	Damping HPF time constant (T_{hpf})	3.1 ms

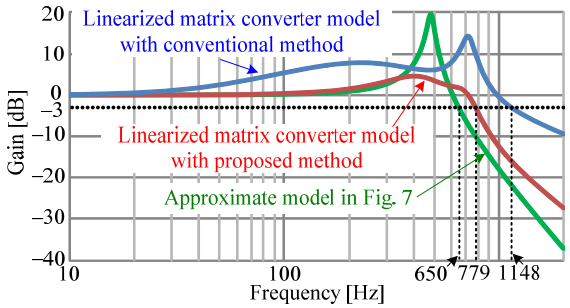

Fig. 10. Gain characteristics of the closed-loop transfer function between $\Delta \boldsymbol{i}_{\mathbf{out}}^*$ and $\Delta \boldsymbol{i}_{\mathbf{out}}$ with the proposed and the conventional methods. The proposed method mitigates the error between the desired and the yielded cut-off frequencies by 1/4 compared to the conventional method.

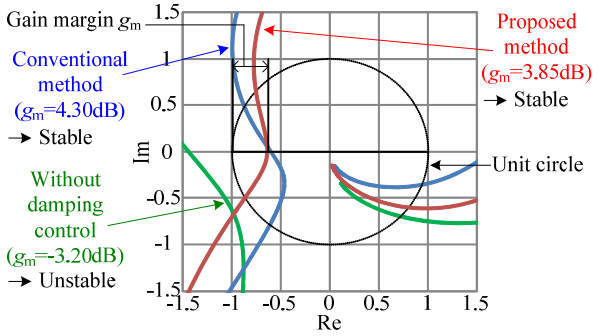

Fig. 11. Nyquist-diagram of the linearized block model of the matrix converter between $\Delta \boldsymbol{i}_{\mathbf{out\_LPF}}^*$ and $\Delta \boldsymbol{i}_{\mathbf{out}}$ with the proposed and the conventional design procedures. The proposed design procedure yields a gain margin of 3.85 dB and the system is stable.

VI. Experimental Results

This chapter evaluates the stability and the transient response of a matrix converter prototype as shown in

Fig.1. The prototype parameters are almost consistent with the parameters shown from Table 1 to Table 4. However, the input voltage is 50 Hz while the output voltage is 30 Hz. In addition, an output d-axis current reference is separated into a steady component of 0.4 p.u. and a step component of 0.05 p.u.. A modulation strategy of the prototype employs the method as introduced in [3].

Fig. 13 shows the input and output waveforms of the matrix converter obtained by experiments. Fig. 13 (a) shows a result without the output damping control and (b) shows a result with the output damping control designed with the proposed method. In Fig. 13 (a), the filter resonance is excited, and the input current and the output current have resonant distortions. It is noted that the experimental result in Fig. 13 (a) shows a stability limit although the simulation result in Fig. 12 becomes unstable. This is because loss of a matrix converter behaves as a damping resistor as mentioned in the previous chapter. The input current THD (total harmonic distortion) is 52.9% and the output current THD is 15.7% from Fig. 13 (a). In contrast, the filter resonance is suppressed and the system is stabilized by the output damping control designed with the proposed method. As a result, the input and output current THDs are reduced to 10.3% and 4.43%, respectively. A main cause of remaining distortion in the input current is generated by commutation failure because the input voltage detection for the commutation is implemented at a power supply not the filter capacitor voltage in the experiment. The input current will be improved by applying a hybrid commutation method [17]. Thus, the designed output damping control mitigates the resonance distortions in the input current by 81%.

Fig. 14 shows the dq-axis output current in a transient response with the damping control designed with the conventional and the proposed methods. It should be noted that the experimental results after this paragraph are obtained in the condition of a fixed output current angle in common with simulations. The conventional and the proposed methods stabilize the matrix converter and the output current converges toward the reference. However, the damping control designed with the conventional method generates a d-axis current overshoot of 188% due to the zero in the closed-loop transfer function. On the other hand, the proposed method reduces the d-axis current overshoot to 76% because of the pole-zero cancellation owing to the proposed reference filter $F(s)$. Hence, the proposed method reduces the output current overshoot in transient response by 60%.

Fig. 15 shows gain curve characteristics of the output current control designed with the proposed and the conventional methods in simulations and experiments. It should be noted that the intended control bandwidth is 650 Hz and the sinusoidal waveform as the d-axis current reference is used in the experiment. The proposed method mitigates the error between the desired and the obtained cut-off frequencies in comparison with the conventional method since the cut-off frequency of the conventional

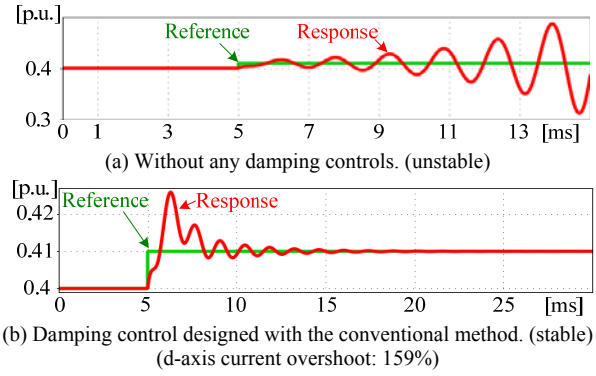

(a) Without any damping controls. (unstable)

(b) Damping control designed with the conventional method. (stable) (d-axis current overshoot: 159%)

(c) Damping control designed with the proposed method. (stable) (d-axis current overshoot: 52.6%)

Fig. 12. Output d-axis current waveform in simulation. The d-axis current overshoot is suppressed by 67 % owing to the proposed method.

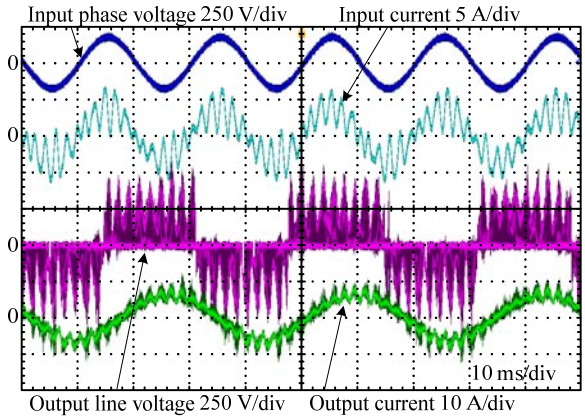

(a) Without the output damping control which results in the input current THD of 52.9%.

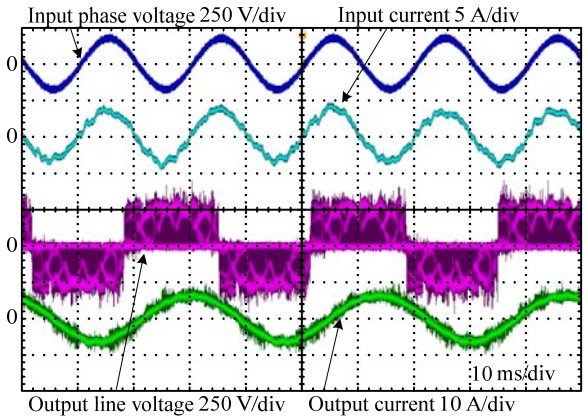

(b) With the output damping control designed with the proposed method which results in the input current THD of 10.3%.

Fig. 13. Input and output waveforms of the matrix converter as illustrated in Fig. 1 in experiments. The output damping control designed with the proposed method suppresses the filter resonance and reduces the input current THD by 81%.

method exceeds 1 kHz because of the damping control. In addition, the proposed method reduces gain in lower frequency band around 100 Hz compared to the conventional method because of the proposed reference filter $F(s)$. As a result, the proposed method reduces the

output current overshoot as shown in Fig. 14. It should be noted that the error between the experimental and the simulation results in Fig. 15 is caused by digital control and a full consideration about the difference will be reported in the future. Therefore, it is confirmed that the proposed design method reduces the output current overshoot and the error of the control bandwidth of the output current.

VII. Conclusion

This paper presents a design procedure for the output current control and the output damping control of a matrix converter to suppress the LC filter resonance and improve a transient response. With the conventional design method, the output damping control causes a large output current overshoot and a control bandwidth of the output current is affected. In the proposed design procedure, a reference filter to suppress an output current overshoot and a design flow chart to obtain a desired control bandwidth of the output current and the stability are proposed. From experimental results, the output damping control designed with the proposed method suppresses the filter resonance, which results in a stable operation. In addition, the proposed design method reduces the output current overshoot of 60% and error between the desired and the obtained control bandwidth in comparison with the conventional method which is based on a gain margin. Therefore, the validity of the proposed design procedure is confirmed.

References

[1] P. W. Wheeler, J. Rodriguez, J. C. Clare, L. Empringham: "Matrix Converters: A Technology Review", IEEE Trans. Ind. Electron., Vol. 49, No. 2, pp. 274-288 (2002)

[2] T. Friedli, J. W. Kolar: "Milestones in Matrix Converter Research", IEEJ Journal I. A., Vol. 1, No. 1, pp. 2-14 (2012)

[3] J. Itoh, I. Sato, A. Odaka, H. Ohguchi, H. Kodachi, N. Eguchi: "A Novel Approach to Practical Matrix Converter Motor Drive System With Reverse Blocking IGBT", IEEE Trans. Power Electron., Vol. 20, No. 6, pp. 1356-1363 (2005)

[4] C. Klumpner, F. Blaabjerg, I. Boldea, P. Nielsen: "New Modulation Method for Matrix Converters", IEEE Trans. Ind. Appl., Vol. 42, No. 3, pp. 797-806 (2006)

[5] F. Blaabjerg, D. Casadei, C. Klumpner, M. Matteini: "Comparison of Two Current Modulation Strategies for Matrix Converters Under Unbalanced Input Voltage Conditions", IEEE Trans. Ind. Electron., Vol. 49, No. 2, pp. 289-296 (2002)

[6] M. Rivera, J. Rodriguez, J. Espinoza, T. Friedli, J. W. Kolar, A. Wilson, C. A. Rojas: "Imposed Sinusoidal Source and Load Currents for an Indirect Matrix Converter", IEEE Trans. Ind. Electron., Vol. 59, No. 9, pp. 3427-3435 (2012)

[7] D. Casadei, G. Serra, A. Tani, L. Zarri: "Stability Analysis of Electric Drives Fed by Matrix Converters", Proc. of the 2002 IEEE-ISIE, Vol. 4, No. 8-11, pp. 1108-1113 (2002)

[8] F. Liu, C. Klumpner, F. Blaabjerg: "A Robust Method to Improve Stability in Matrix Converters ", Proc. 35th PESC 2004, pp. 3560-3566 (2004)

[9] C. A. J. Ruse, J. C. Clare, C. Klumpner: "Numerical Approach for Guaranteeing Stable Design of Practical Matrix Converter Drive Systems", Proc. 32nd IECON 2006, pp. 2630-2635 (2006)

[10] D. Casadei, G. Serra, A. Tani, A. Trentin, L. Zarri: "Theoretical and Experimental Investigation of the Stability of Matrix Converters", IEEE Trans. Ind. Electron., Vol. 52, No. 5, pp. 1409-1419 (2005)

[11] Y. Sun, M. Su, X. Li, H. Wang, W. Gui: "A General Constructive Approach to Matrix Converter Stabilization", IEEE Trans. Power Electron., Vol. 28, No. 1, pp. 418-431 (2013)

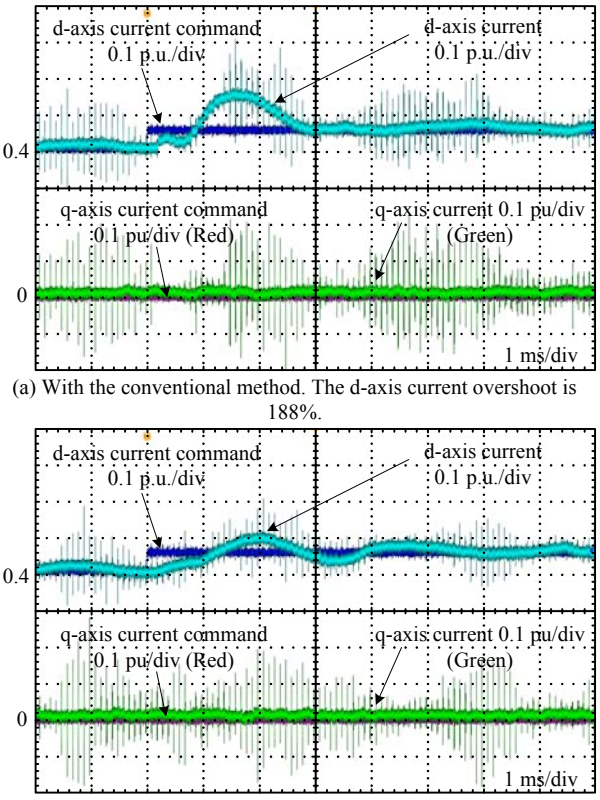

(a) With the conventional method. The d-axis current overshoot is 188%.

(b) With the proposed method. The d-axis current overshoot is 76%.

Fig. 14. Output dq-axis current response with the damping control designed with the conventional and the proposed methods. The proposed method reduces the current overshoot in transient response by 60%.

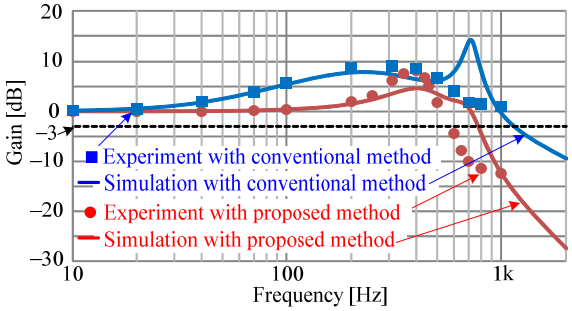

Fig. 15. Gain characteristics of the closed-loop transfer function between Δi_{out}^* and Δi_{out} with the proposed and the conventional methods in simulation and experiment.

[12] M. Rivera, C. Rojas, J. Rodriguez, P. W. Wheeler, B. Wu, J. Espinoza: "Predictive Current Control With Input Filter Resonance Mitigation for a Direct Matrix Converter", IEEE Trans. Power Electron., Vol. 26, No. 10, pp. 2794-2803 (2011)

[13] T. Nunokawa, T. Takeshita:"Resonance Suppression Control in Complex Frame for Three-Phase to Three-Phase Matrix Converters", EPE2007 (2007)

[14] J. Haruna, J. Itoh: "Control Strategy for a Matrix Converter with a Generator and a Motor", Proc. 26th IEEE APEC, pp. 1782-1789 (2011)

[15] H. Takahashi, J. Itoh: "Stability Analysis of Damping Control to Suppress Filter Resonance in Multi-modular Matrix Converter", IEEE Energy Conversion Congress and Expo 2013, pp. 448-455 (2013)

[16] D. Casadei, G. Serra, A. Tani, L. Zarri: "Matrix Converter Modulation Strategies: Anew General Approach Based on Space-Vector Representation of the Switch State", IEEE Trans. Ind. Electron., Vol. 49, No. 2, pp. 370-381 (2002)

[17] K.Kato, J. Itoh: "Improvement of Input Current Waveforms for a Matrix Converter Using a Novel Hybrid Commutation Method", Proc. PCC 2007, pp. 763-768 (2007)